UNIVERSITY of CALIFORNIA
SANTA CRUZ

EXTRACTION OF EFFECTIVE DOPING CONCENTRATIONS IN UN-IRRADIATED AND IRRADIATED SILICON DETECTORS

A thesis submitted in partial satisfaction of the
requirements for the degree of

BACHELOR OF SCIENCE

in

PHYSICS

by

Christopher Betancourt

19 March 2009

The thesis of Christopher Betancourt is approved by:

Professor Hartmut F. -W. Sadrozinski
Technical Advisor

Professor Glenn Alers
Technical Advisor

Professor David P. Belanger
Thesis Advisor

Copyright © by

Christopher Betancourt

2009

Contents

List of Figures iv

List of Tables vi

Dedication vii

Acknowledgements viii

1 Introduction 1

1.1 Silicon Detectors 1

1.2 Experimental Set-Up 3

2 Un-irradiated Detector Model 4

3 Un-Irradiated Detector Results 7

4 Irradiated Detector Model 11

4.1 Basic Semiconductor Equations 11

4.2 Equilibrium Requirements 13

4.3 Steady State Requirements 14

4.4 Depletion Depth and the Debey Length 15

4.5 Conductance and Capacitance Measurements 16

4.6 Extraction of Trap Parameters from the Admittance 21

5 Irradiated Detector Results 24

6 Conclusions and Summary 29

Bibliography 32

List of Figures

1.1 Top down view of a Silicon Strip detector 1
1.2 Cross section view of a silicon strip detector 2
1.3 Illustration showing electron-hole pair generation from an ionizing particle. The charge carriers are collected by the Al strips and carried to the readout electronics 2

2.1 Coordinate view within a strip detector. The x axis represents the coordinate across the detector while the y axis is in the direction of the depth of the detector 5
2.2 A 2-D potential solution for a strip detector determined from the appropriate boundry conditions 5

3.1 Measured and Simulated $1/C^2(V)$ curves for a strip detector 8
3.2 Extracted Doping density in the y direction 8
3.3 $1/C^2$ curves for a strip detector and diode showing the effect of the strip geometry on the depletion voltage. The offset is seen in the "foot" 9
3.4 A closer look at the "foot" displaying the effect of different geometries on capacitance measurements 9
3.5 Theoretical values of the voltage range of the "foot" for two different geometries determined from the 2-D potential solution 10

4.1 The four processes involved in generation and recombination through a deep defect at energy E_t: a.) emission of an electron into the conduction band, b.) capture of an electron from the conduction band, c.) capture of a hole from the valence band, d.) emission of a hole into the valence band. 14
4.2 Energy band diagram for a junction containing deep level with the corresponding equivalent circuit. The generation/recombination contribution to the admittance of each deep level can be modeled as a capacitor and resistor in series 18
4.3 Measured and simulated C and G/ω as a function of frequency taken at 100V. Simulation assumed two main trap levels. 22
4.4 Measured and simulated C and G/ω as a function of frequency taken at 200V. The low frequency capacitance measurement is lower than expected 23

5.1 Extracted depletion region depth of a p-on-n FZ diode irradiated to 4.2E+14 pions/cm^2 and Median Charge of a p-on-n FZ strip detector irradiated to 6.0E+14 pions/cm^2. Also included is the depth calculated using the 10kHz capacitance. 25

5.2 Extracted depletion region depth of a n-on-p MCz diode irradiated to 5E+14 neutrons/cm^2 and Median Charge of a n-on-p MCz strip detector irradiated to 5E+14 neutrons/cm^2 25

5.3 Depletion region depth as a function of voltage for neutron irradiated detectors, calculated using equation (4.34) 26

5.4 Depletion region depth as a function of voltage for pion irradiated detectors, calculated using equation (4.34) 26

5.5 Arrhenius Plot for the dominant trap level. Activation energy was found to be E=.547 eV below the conduction band 27

List of Tables

5.1 Deep Level Parameters 28

Dedicated to my father,

Luis Betancourt

Acknowledgements

I first want to thank my mother, Victoria Betancourt, who put me through college and never stopped believing and encouraging me. Ford Hurley, whose previous work was the precursor to this paper, for always being there to help in the lab and for helping get the data needed to make the analysis. Mark Gerling for taking virtually all the admittance measurements. Sulimon Sattari for helping with the analysis. Forest Martinez-McKinney for his help mounting and bonding detectors. I would also like to thank the rest of the people at SCIPP for making me feel welcome into their community. There are two people I would especially like to thank, as this paper would not have been possible without them; Glenn Alers who helped the most with the theoretical framework of this paper and Hartmut Sadrozinski for giving me the incredible opportunity to work on this topic and for pushing me to do my best.

1 Introduction

1.1 Silicon Detectors

High energy particle physics requires not only a sophisticated theoretical framework, but also the latest and most advanced engineering technology. In order to create and track high energy particles, huge particle accelerators must smash together beams of matter and antimatter at speeds close to the speed of light. When the beams collide, a shower of high energy particles shoot off from the collision point. In elementary particle physics experiments silicon is regarded as the best material choice for detecting high energy particles. The inner detector of the ATLAS experiment at the Large Hadron Collider will employ several of these silicon detectors.

Silicon detectors, shown in Figure 1.1, are semiconductor devices which are used to detect high energy particles. They are complicated diode devices containing p-n junctions, as seen in Figure 1.2. When a voltage is applied to the device, the mobile free carriers are swept from the device leaving an area known as the space charge region which is where the active electric field

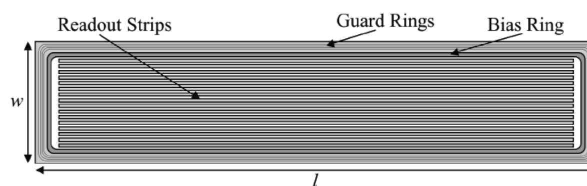

Figure 1.1: Top down view of a Silicon Strip detector

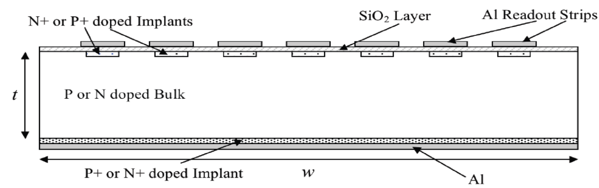

Figure 1.2: Cross section view of a silicon strip detector

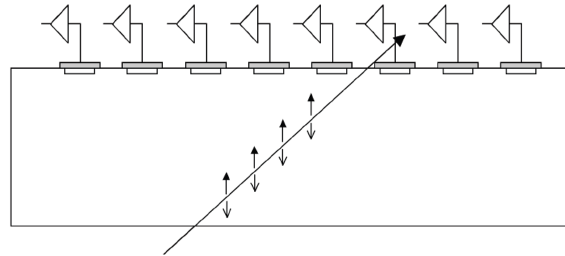

Figure 1.3: Illustration showing electron-hole pair generation from an ionizing particle. The charge carriers are collected by the Al strips and carried to the readout electronics

of the device can be found. A high energy particle passing through a silicon detector will create electron/hole pairs along its path, as shown in Figure 1.3. Under the influence of an electric field, these liberated charges will travel to the aluminum readout strips of the detector, amplified and then sent to readout electronics. Because the detector is arranged in strips, a high energy particle's position can be determined with very hig resolution when it passes through a detector.

Due to their proximity to the collision point, silicon detectors at ATLAS will be exposed to high amounts of radiation. Radiation will damage the detector in a number of ways. One of the largest effect is an increase in the leakage current, causing irradiated detectors to become very noisy unless operated at low temperatures. The other noticeable effect is a change in the space-charge density of the device. This will cause a change in the depletion voltage, so that highly irradiated detectors must be operated at very high voltages. For this reason, the study of radiation damage in silicon detectors is very important for the longevity of silicon detectors at the LHC.

1.2 Experimental Set-Up

Admittance measurements have been performed on silicon pad detectors produced of both p-on-n and n-on-p and FZ and MCz material. The un-irradiated sensors were produced by MICRON at Sussex, UK, on 300μm FZ wafers of about 20kΩcm resistivity and MCz wafers of about 2kΩcm resistivity and by Hamamatsu Photonics (HPK) at Hamamatsu City, Japan, on 330μm FZ wafers of about resistivity. The neutron irradiation was performed at Ljubljana and pion irradiation was performed at PSI in Switzerland.

The charge collection and C-V measurements on microstrip detectors have been performed at SCIPP, UC Santa Cruz. The CCE(V) investigations have been carried out with a 90Sr beta source, described in [1]. CCE(V) measurements were taken up to 1100V. The Admittance experimental set-up is based on a HP 4284A LCR meter coupled with the HP 16065A text fixture (modified to permit biasing with voltages up to 700 V). Voltage sourcing and current monitoring are performed through a computer controlled Keithley 2410 HV supply. In order to reduce the leakage current noise, CCE(V) taken at -20 ^{o}C. More details on the experimental system for CCE(V) are given in [2].

The temperature was varied in between admittance measurements, ranging from 0 ^{o}C up to 20 ^{o}C in 5 ^{o}C steps. During each measurement, the temperature was kept constant using a cooling set-up that included peltiers for cooling, and liquid nitrogen gas boil off to remove moisture from the air so no ice forms on the detectors. Several frequencies, ranging from 100 Hz to 2 MHz, of the AC signal imposed by the LCR meter were cycled through at the beginning of each new voltage run. Admittance measurements were only taken up to 630V and for detectors that did not deplete before this, the depletion voltage was taken from previous data on corresponding detectors. Simulations were produced assuming two dominant deep levels, although one deep level was clearly more dominant than the other.

2 Un-irradiated Detector Model

The extraction of the doping concentrations is fairly straightforward in un-irradiated detectors. Shallow dopants are fully ionized at room temperature, and the leakage current has a negligible effect on the electric field in the device. This reduces the extraction of doping concentrations to a simple electrostatics problem, where thermal effects can be neglected. Due to the simplicity of the problem, a solution incorporating the geometry of a given detector , shown in Figure 2.1, can be included.

In un-irradiated detectors, $1/C^2(V)$ curves are used to extract the doping density of a detector. Starting with Poisson's equation in two dimensions

$$\nabla^2 V(x,y) = -\frac{qN_{eff}(y)}{\epsilon} \tag{2.1}$$

subject to the following boundry conditions [3]

$$\begin{aligned} V(x,y) &= V(x+p,y) && (2.2)\\ V(x,0) &= V_{bias},\ |x| \geq (p-w)/2 && (2.3)\\ V(x,d) &= 0 && (2.4)\\ \frac{\partial}{\partial y}V(x,y)\Big|_{y=0} &= 0,\ |x| \leq (p-w)/2 && (2.5) \end{aligned}$$

where x is the coordinate across the detector, y the coordinate in the direction of the depth, d is the depleted depth, p and w are the pitch and width of the detector respectively.

An analytic solution to these equations is shown in Figure 2.2. These boundary conditions only incorporate the geometry of the detector and do not deal with special cases such as p-spray or

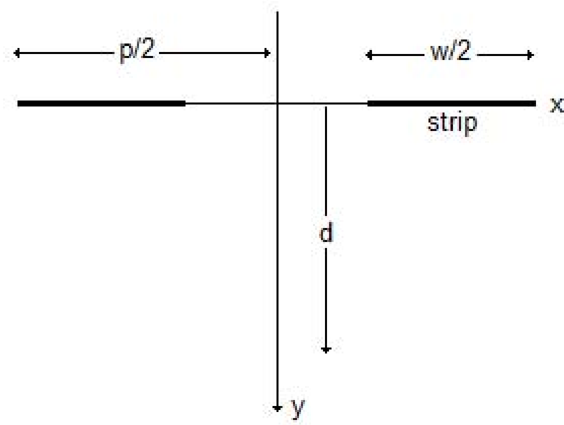

Figure 2.1: Coordinate view within a strip detector. The x axis represents the coordinate across the detector while the y axis is in the direction of the depth of the detector

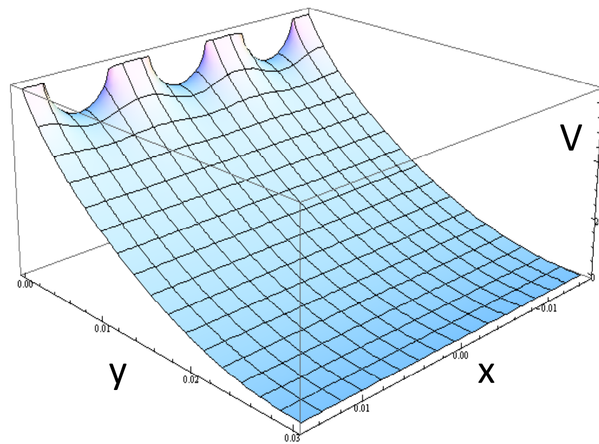

Figure 2.2: A 2-D potential solution for a strip detector determined from the appropriate boundry conditions

p-stop that may be present in some detectors. For these cases, a numerical approach is needed. In [4], a 2D numerical solution is developed based on finite difference methods, and can be modified to incorporate such special cases mentioned above.

3 Un-Irradiated Detector Results

In order to simulate C-V curves we introduce an additional boundry condition,

$$\frac{\partial}{\partial y} V(x,y)\Big|_{y=d} = 0 \tag{3.1}$$

This will allow one to calculate V_{bias} given a trial doping density N_{eff} and depleted depth d. This can be combined with the equation for a parallel plate capacitor

$$C = \epsilon \frac{A}{d} \tag{3.2}$$

where ϵ is the permittivity of silicon and A is the area of the detector.

$1/C$ and $1/C^2$ voltage curves can be simulated by varying d and $N_{eff}(y)$ is then adjusted until the simulated C-V curve matches the measured C-V curve. A plot of measured and simulated $1/C^2(V)$ curves, along with the extracted $N_{eff}(y)$ that would reproduce such a curve for a n-on-p-type Float Zone (FZ) detector of thickness $300\mu m$, are shown in Figure 3.1 and Figure 3.2 respectively. The simulation extracts a reasonable doping density and reproduces the p+ layer that is expected near the backplane of the detector.

By comparing the C-V curves of a diode with that of a strip detector of the same wafer, it can be seen that the strips seem to offset the curves by a small amount, and thus increase the depletion voltage. Figure 3.3 shows the increase in depletion voltage due to the strips that can be seen as an offset in $1/C^2(V)$ curves at low voltage, compared to a diode where no offset is observed. This offset in the curves is colloquially referred to as the "foot", and is defined as the difference between the depletion voltage of a diode and strip detector of the same type. Figure 3.4 shows $1/C(V)$

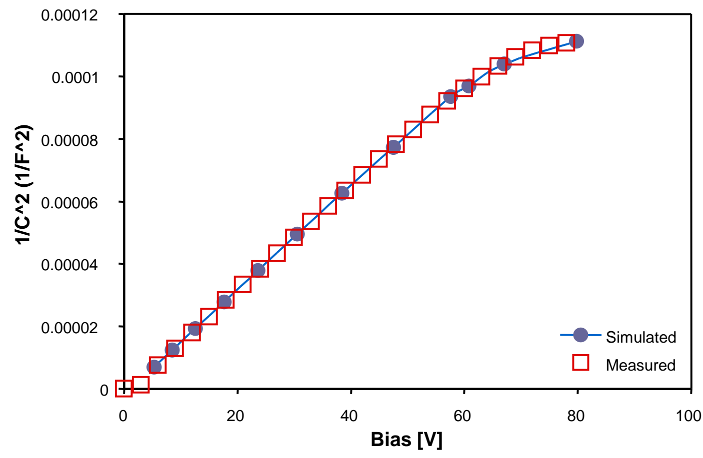

Figure 3.1: Measured and Simulated $1/C^2(V)$ curves for a strip detector

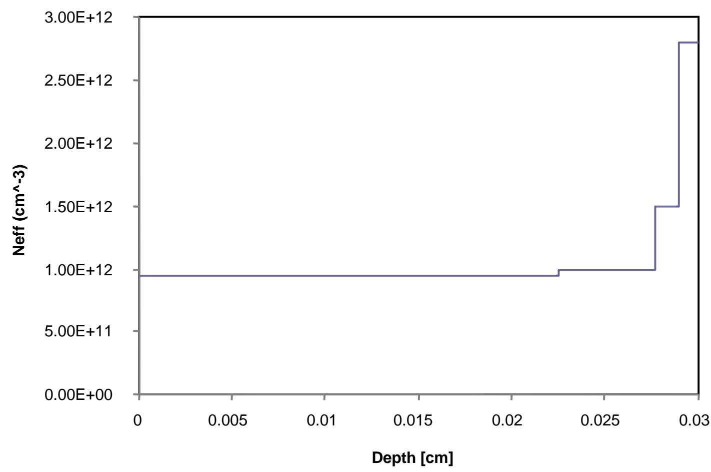

Figure 3.2: Extracted Doping density in the y direction

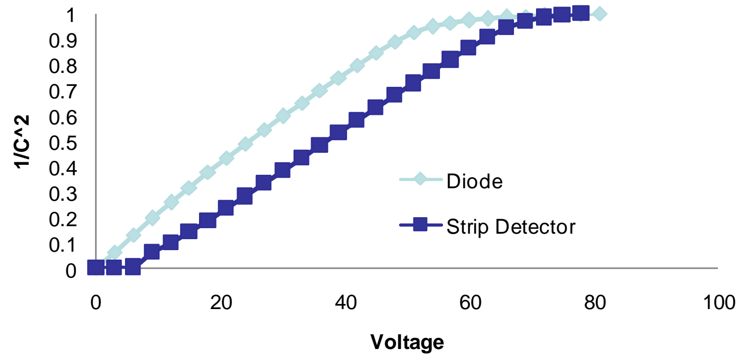

Figure 3.3: $1/C^2$ curves for a strip detector and diode showing the effect of the strip geometry on the depletion voltage. The offset is seen in the "foot"

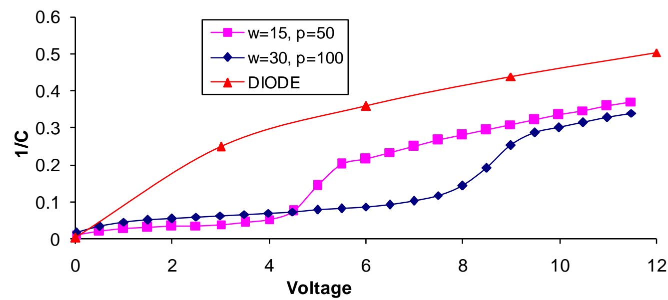

Figure 3.4: A closer look at the "foot" displaying the effect of different geometries on capacitance measurements

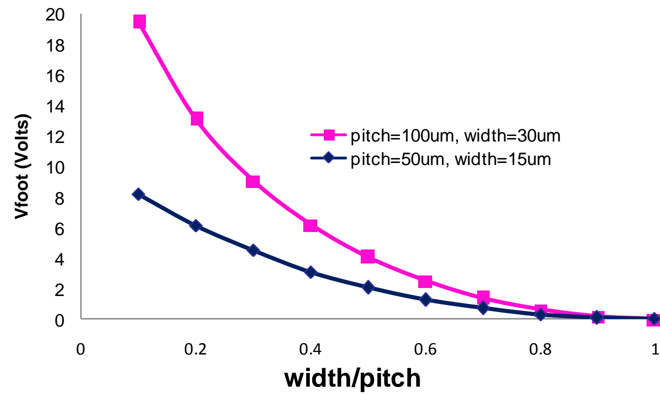

Figure 3.5: Theoretical values of the voltage range of the "foot" for two different geometries determined from the 2-D potential solution

displaying how the "foot" changes with pitch and strip width. The 2-D solution for the potential predicts an increase to the depletion voltage due to the strips of the detector. By assuming that the increase in depletion voltage is the same as the voltage range of the "foot", we can predict the voltage range of the "foot" by varying the pitch and strip width. The predicted voltage range of the "foot" for detectors of different pitch and strip width is shown in Figure 3.5. The theory correctly predicts the effect of the pitch and strip width on the voltage range of the "foot".

4 Irradiated Detector Model

Radiation damage creates defects, or traps, in the band gap that alter detector properties. In the space charge region, these defects are responsible for the generation and trapping of the leakage current. It is trapping of the leakage current that leads to a steady state filling of the defects by free charge carriers in the space charge region of an irradiated detector. In the undepleted bulk, charge neutrality approximately holds and the bulk can be treated as being in thermal equilibrium, where the leakage current does not influence the filling of traps.

There are two types of defect states. *Donors* are defects that are charged when occupied by holes, and neutral when occupied by electrons. *Acceptors* are defects that are neutral when occupied by holes, and charges when occupied by electrons. The occupancy of defects in thermal equilibrium is governed by the Fermi level, while in a steady state the occupancy is governed by the free carrier concentrations in the conduction and valence bands.

4.1 Basic Semiconductor Equations

In order to determine the doping profile in irradiated detectors, the following basic equations for a semiconductor with an arbitrary number of defects must be satisfied [5].

The Electric Field is given by Poisson's equation,

$$\frac{d}{dx}E(x) = \frac{q}{\epsilon}\left(N_{dopant} + \sum_{Donors} p_t(x) - \sum_{Acceptors} n_t(x)\right) \tag{4.1}$$

where N_{dopand} is the initial concentrations before irradiation, n_t and p_t are the concentration of trapped electrons and holes respectively, for a trap with concentration N_t at an Energy E_t. Neglecting diffusion and tunneling effects, the current is defined by,

$$j = j_n + j_p \tag{4.2}$$

where,

$$j_n = q\mu_n n(x)E(x) \tag{4.3}$$

$$j_p = q\mu_p p(x)E(x) \tag{4.4}$$

are the electron and hole current components. Here $\mu_{n,p}$ represents the mobility of electrons and holes respectively, q is the elementary charge of the electron, and $n(x)$, $p(x)$ are the free carrier concentrations. The current must also satisfy

$$\frac{d}{dx}j = 0 \tag{4.5}$$

Combining equations (4.2) and (4.5) we get,

$$\frac{d}{dx}j_n = -\frac{d}{dx}j_p \tag{4.6}$$

The continuety equations for a semiconductor are,

$$\frac{\partial n}{\partial t} = U_n + \frac{1}{q}\frac{d}{dx}j_n \tag{4.7}$$

$$\frac{\partial p}{\partial t} = U_p - \frac{1}{q}\frac{d}{dx}j_p \tag{4.8}$$

where U_e and U_h are the net electron and hole generation/recombination rates and are given by,

$$U_n = \sum_{traps} e_{n,t}n_t - nc_{n,t}p_t \tag{4.9}$$

$$U_p = \sum_{traps} e_{p,t}p_t - pc_{p,t}n_t \tag{4.10}$$

where e_n, e_p are the emission rates and c_n, c_p are the capture probabilities for electrons and holes respectively and are defined by,

$$e_{n,p} = c_{n,p} N_{c,v} e^{\mp(E_{c,v}-E_t)/kT} \tag{4.11}$$

$$c_{n,p} = v_{n,p}^{th} \sigma_{n,p} \tag{4.12}$$

where $N_{c,v}$ is the density of states in the conduction and valence bands, $v_{n,p}^{th}$ is the thermal velocity of free carriers and $\sigma_{n,p}$ is the capture cross section for electrons and holes respectively.

4.2 Equilibrium Requirements

In thermal equilibrium, the occupancy of defect levels is given by Boltzmann's statistics. Here, the Fermi Energy dictates the filling of defect levels. The probability of the occupancy of a band orbital at an energy E is given by the Fermi-Dirac distribution,

$$f_e = \frac{1}{1 + e^{(E-E_f)/kT}} \tag{4.13}$$

where E_f is the Fermi Energy.

The probability of defects is not simply given by the Fermi-Dirac distribution. A *Donor* state can be occupied by an electron of either spin up or down, so there are two orbital at the same energy. The difference from band oribitals arises because once an electron is bound to a *Donor* state, that state cannot take on another electron of opposite spin. The probability that a *Donor* at energy E_D is occupied by electron is given by

$$f_D = \frac{1}{1 + \frac{1}{2} e^{(E_D-E_f)/kT}} \tag{4.14}$$

and occupied by a hole by

$$f_D{}^+ = \frac{1}{1 + 2e^{(E_f-E_D)/kT}} \tag{4.15}$$

The probability that an *Acceptor* at energy E_A is occupied by an electron is slightly different and is given by

$$f_A{}^- = \frac{1}{1 + 2e^{(E_A-E_f)/kT}} \tag{4.16}$$

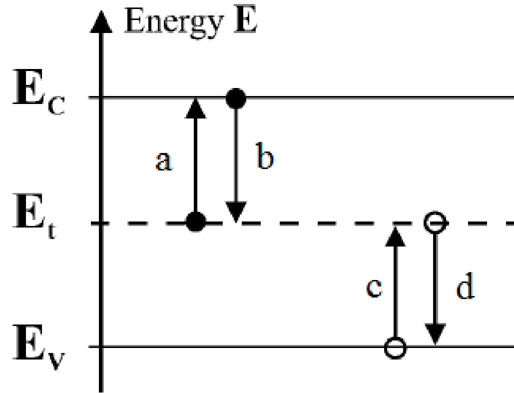

Figure 4.1: The four processes involved in generation and recombination through a deep defect at energy E_t: a.) emission of an electron into the conduction band, b.) capture of an electron from the conduction band, c.) capture of a hole from the valence band, d.) emission of a hole into the valence band.

and for holes

$$f_A = \frac{1}{1 + \frac{1}{2}e^{(E_f - E_A)/kT}} \tag{4.17}$$

Charge neutrality requires that

$$n + \sum_{Acceptors} f_A{}^- N_t = p + \sum_{Donors} f_D{}^+ N_t \tag{4.18}$$

which just states that the total number of trapped and free electrons is equal to the total number of trapped and free holes in our device.

4.3 Steady State Requirements

The occupancy of defects under steady state conditions is determined from Shockley Read Hall (SRH) statistics. Each defect can emit and capture electrons from the conduction band, as well as emit or capture holes from the valence band. These four competing processes, shown in Figure 4.1 determine the steady state filling of traps. The number of trapped charge carriers for a given defect can be determined from the steady state requirements. For a given defect, the

concentration of trapped electrons plus the concentration of trapped holes must equal concentration of the defect, which gives

$$N_t = n_t + p_t \tag{4.19}$$

Under steady state, equations (4.7) and (4.8) become,

$$\frac{\partial n}{\partial t} = U_e + \frac{1}{q}\frac{d}{dx}j_e = 0 \tag{4.20}$$

$$\frac{\partial p}{\partial t} = U_h - \frac{1}{q}\frac{d}{dx}j_h = 0 \tag{4.21}$$

Combining (4.20) and (4.21) and inserting (4.6) gives,

$$U_e = U_h \tag{4.22}$$

i.e. the net generation/recombination rates for electrons and holes must be equal. This is the necessary condition which must be satisfied under a steady-state. The number of trapped charge carriers can be determined from inserting in equations (4.9), (4.10), and (4.19) into (4.22), resulting in,

$$n_t = N_t f_s = N_t \frac{c_n n(x) + e_p}{c_n n(x) + e_n + c_p p(x) + e_p} \tag{4.23}$$

where f_s is the occupancy of electrons under a steady state.

4.4 Depletion Depth and the Debey Length

There are three main regions in biased detector; the depletion or space charge region, the undepleted bulk, and the transition region between these two areas whose length is given by the Debey Length. In unirradiated devices, the debey length is essetially zero, and the trasition between depleted and undepleted bulk is abrupt. In irradiated devices, the free carrier concentration at the edge of the space charge region is changed, causing a change in the Debey length.

The transition region is characterized by the Debey length. The electric field will not just disappear at the depletion layer edge, but will gradually dissipate into the undepleted region. It

has to do with the fact that at the edge of the depletion region, there are free carriers that have yet to be swept from the detector. These free carriers act as a shield for the undepleted region from the electric field present in the space charge region. The larger the number of free carriers, the more shielding there is, leading to a smaller transition region. If the free carrier concentration is small, then they will shield the undepleted bulk less, which would lead to a larger transition region. At about one Debey length away from the depleted region, the electric field is very small, and we can think of the region beyond this to have zero electric field. The rest of the detector past the Debey length can then be treated as undepleted neutral bulk.

The maximum depletion depth of the detector will be limited by the Debey length. As the bias voltage is increased, the neutral undepleted bulk will shrink. Once the length of this region hits zero, then one cannot deplete the detector any more. What is left is the space charge region and the transition region. So the maximum depth of the space charge region is given by,

$$d_{max} = W - L_D \tag{4.24}$$

where W is the total thickness of the detector and L_D is the Debey length. The Debey length can be determined from the flatband capacitance by [7],

$$C_f = A\left(\frac{\epsilon q^2 n_f}{kT}\right)^{1/2} = \epsilon A/L_D \tag{4.25}$$

where A is the area of the detector, and n_f is the free carrier concentration at the depletion layer edge. Admittance measurements are used to determine C_f and thus L_D.

4.5 Conductance and Capacitance Measurements

When a reversed bias voltage is applied to a detector, mobile charge carriers are swept from the device, creating an active region called the space charge region with a thickness d. By superimposing a small AC voltage on top of the bias voltage, the vicinity of d can be examined. Each trap level will interact with the AC voltage differently depending on the lifetime of the trap.

The defects will only be active when the frequency of the AC signal corresponds to the emission rate of the defects. At high frequencies, the defect levels will not have enough time to respond to the signal, and at very low frequencies all defects will be active.

Consider the vicinity of the depletion layer edge at d. Deep defect levels will cross the Fermi Energy of the bulk at a distance x_t, as illustrated in Figure 4.2. At x_t, the occupancy of the level will change from its equilibrium value to its steady state value in the space charge region which is given in the previous section. The AC signal imposed on the detector will give rise to a frequency dependent complex capacitance as the occupancy of the defect switches between its equilibrium value and its value in the space charge region. Since the minority free carrier density is much smaller than the majority free carrier density, we can neglect minority carrier response to the AC signal in the bulk. In order to recieve the signal produced by generation/recombination of the deep levels, the frequency must be such that there is sufficient time for the deep level to emit free charge carriers. The relaxation time associated with this level for n-type material is given by [6][7],

$$\tau_t = [2e_{n,t}]^{-1} \tag{4.26}$$

and for p-type

$$\tau_t = [2e_{p,t}]^{-1} \tag{4.27}$$

Consider the complex admittance, Y, of the device where the series resistance and capacitance are turned into a conductor and capacitor in parallel,

$$Y = Z^{-1} = G_p + j\omega C_p \tag{4.28}$$

where G_p and C_p are the conductance and capacitance in parallel to each other. The complex admittance can be used to determine trap parameters such as lifetimes, Energies, capture cross sections, and concentrations. In order to model the contribution to the conductance and capacitance, an equivalent circuit model taking into account the contribution of generation-recombination and crossover capacitance to the admittance must be used. An equivalent circuit for bulk trap

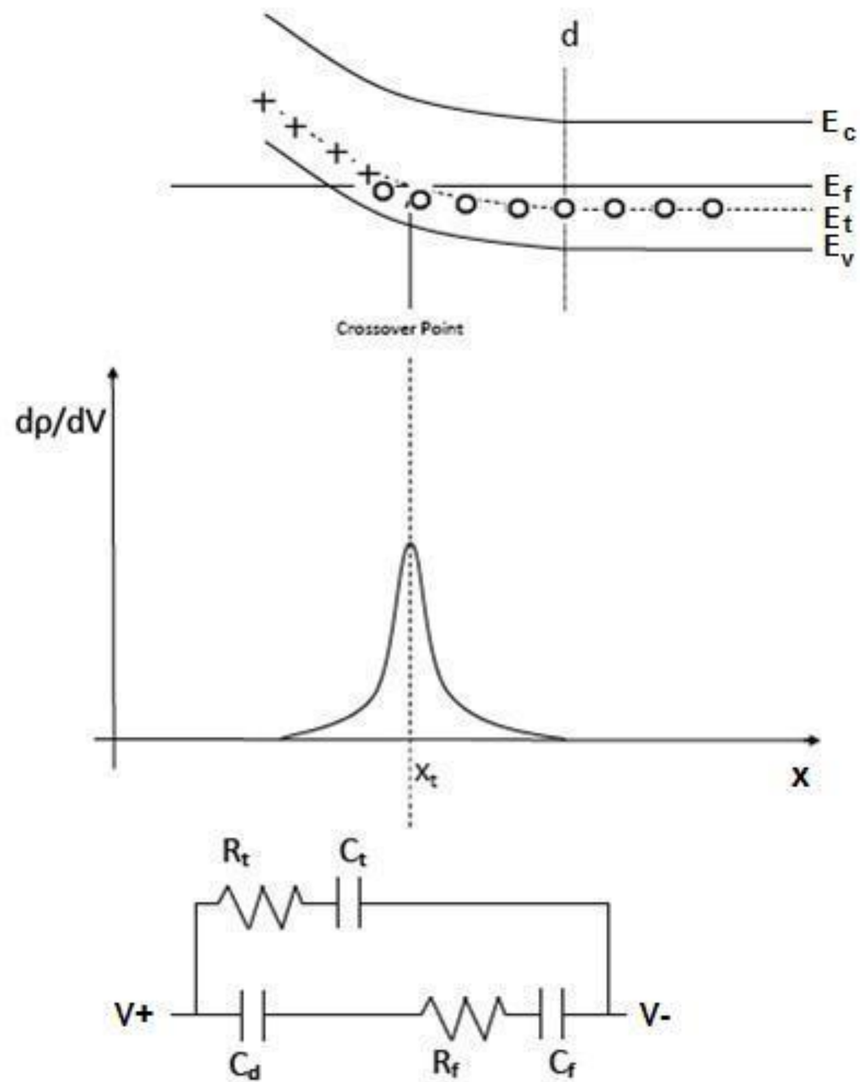

Figure 4.2: Energy band diagram for a junction containing deep level with the corresponding equivalent circuit. The generation/recombination contribution to the admittance of each deep level can be modeled as a capacitor and resistor in series

contribution to the admittance is derived in both [6][7]. In this model, G_p/ω and C_p are given by,

$$G_p/\omega = \sum_{t=1}^{N} C_{bt} \frac{ln(1+(\omega\tau_t(1-f_s))^2)}{2\omega\tau_t(1-f_s)} \tag{4.29}$$

and

$$C_p = C_{hf} + \sum_{t=1}^{N} C_{bt} \frac{tan^{-1}(\omega\tau_t(1-f_s))}{\omega\tau_t(1-f_s)} \tag{4.30}$$

where C_{hf} is the high frequency capacitance given by [7][8],

$$C_{hf} = (1/C_d + 1/C_f)^{-1} \tag{4.31}$$

where C_d is the capacitance of the space charge region and C_f is the flatband capacitance associated with the Debey length. C_{bt} is the capacitance of the number of active bulk trap levels within a few kT of the crossover and is given by [3],

$$C_{bt}(V) = \frac{\sqrt{2}C_d(V)N_{act}}{N_d}(1 - v_t/u_f)^{-1/2} \tag{4.32}$$

where v_t and u_f are the energies of the trap level and bulk Fermi level measured from the midgap, N_{act} is the density of active or charges defects and N_d is the original dopant density. We take the capacitance at depletion to be

$$C_d(V_{dep}) = \epsilon A/(W - L_d) \tag{4.33}$$

where W is the width of the detector. If we combine equations (4.32) and (4.33) then we find

$$d = \frac{C_{bt}(V_{dep})}{C_{bt}(V)}(W - L_d) \tag{4.34}$$

which gives the depleted depth of an irradiated silicon detector. The frequency ω_p where the G_t/ω curve is peaked is given by,

$$\omega_p\tau_t(1-f_s) = 1.98 \tag{4.35}$$

While this model reproduces the general form of our data, it fails to give a quantitative fit. The measured curves are broader than predicted. Our model must be modified to quantitatively describe our conductance and capacitance curves.

The model presented above can be extended by including a dispersion of trap lifetimes [6]. There are two models that have been proposed to include time constant dispersion; one incorporates a fluctuation of band bending at the depletion layer edge caused by a random distribution of point charges located at the surface, and the other incorporates a distribution of capture probabilities caused by the chemical environment near the defect sites. The former will be used in this paper to account for time constant dispersion.

Consider a random spatial distribution of point charges located at the surface of the detector. This non-uniform spatial distribution of charge will lead to a spatial variation of the band bending at the depletion layer edge. This variation in band bending will result in different response times from the defect levels near the depletion layer edge. This will then lead to a dispersion of time constants that is related to the amount of band bending variation. By integrating over all possible band bending values, the conductance and capacitance contribution of a trap state to include band bending variation is given by [6],

$$G_t(\omega)/\omega = \frac{C_{bt}(2\pi{\sigma_s}^2)^{-1/2}}{2\xi}\int_{-\infty}^{\infty} exp\left(-\frac{\eta^2}{2{\sigma_s}^2}\right) exp(-\eta) ln(1+\xi^2 exp(2\eta))d\eta \tag{4.36}$$

and

$$C_t(\omega) = \frac{C_{bt}(2\pi{\sigma_s}^2)^{-1/2}}{\xi}\int_{-\infty}^{\infty} exp\left(-\frac{\eta^2}{2{\sigma_s}^2}\right) exp(-\eta) tan^{-1}(\xi exp(\eta))d\eta \tag{4.37}$$

where ${\sigma_s}^2$ is called the variance of band bending, and $\xi = \omega\tau_t(1-f_s)$. Here σ_s and C_{bt} are taken to be free parameters and are extracted from G_p/ω curves. Once σ_s is known, the lifetime τ_t is given by

$$\xi_p = \omega_p\tau_t(1-f_s) \tag{4.38}$$

where the ξ_p is determined by,

$$\int_{-\infty}^{\infty} exp\left(-\frac{\eta^2}{2{\sigma_s}^2}\right) exp(-\eta)\left(\frac{2\xi_p exp(2\eta)}{1+{\xi_p}^2 exp(2\eta)} ln(1+\xi^2 exp(2\eta))\right) d\eta = 0 \tag{4.39}$$

which can be solved numerically. It should be pointed out that when the bias voltage is increased, the depletion layer edge will move further away from the surface. This will cause surface effects to

diminish as the voltage is increased. As a result, we expect the variance of band bending, σ_s will tend to zero at sufficiently high voltages. The total conductance of our device is given by,

$$G_p(\omega)/\omega = \sum_{traps} G_t(\omega)/\omega \tag{4.40}$$

and the capacitance by,

$$C_p(\omega) = C_{hf} + \sum_{traps} C_t(\omega) \tag{4.41}$$

4.6 Extraction of Trap Parameters from the Admittance

The energy of each trap level can be determined from the temperature dependence of the peak frequency, ω_p. We know that,

$$\omega_p = \xi/\tau_t = \xi 2 c_{n,p} N_{c,v} exp[\mp(E_{c,v} - E_t)/kT] \propto T^2 exp[\mp(E_{c,v} - E_t)/kT] \tag{4.42}$$

If we take measurements at temperatures T_1 and T_2, and find peaks at ω_1 and ω_2 respectively, we can then write,

$$E_a = k\left(\frac{T_1 T_2}{T_1 - T_2}\right) ln\left(\frac{\omega_1}{\omega_2}\left(\frac{T_2}{T_1}\right)^2\right) \tag{4.43}$$

where $E_a = \pm(E_{c,v} - E_t)$ is activation energy of the trap level taken with respect to the majority carrier band edge. Once the trap energy and majority carrier emission rate is known, the majority carrier capture cross section can be calculated using equations (4.11) and (4.12).

The density of charged traps, N_{act}, can be determined by adjusting C_{bt} so that simulated curves fits of measured curves. Once C_{bt} is known, equation (4.32) can be used to determine N_{act}.

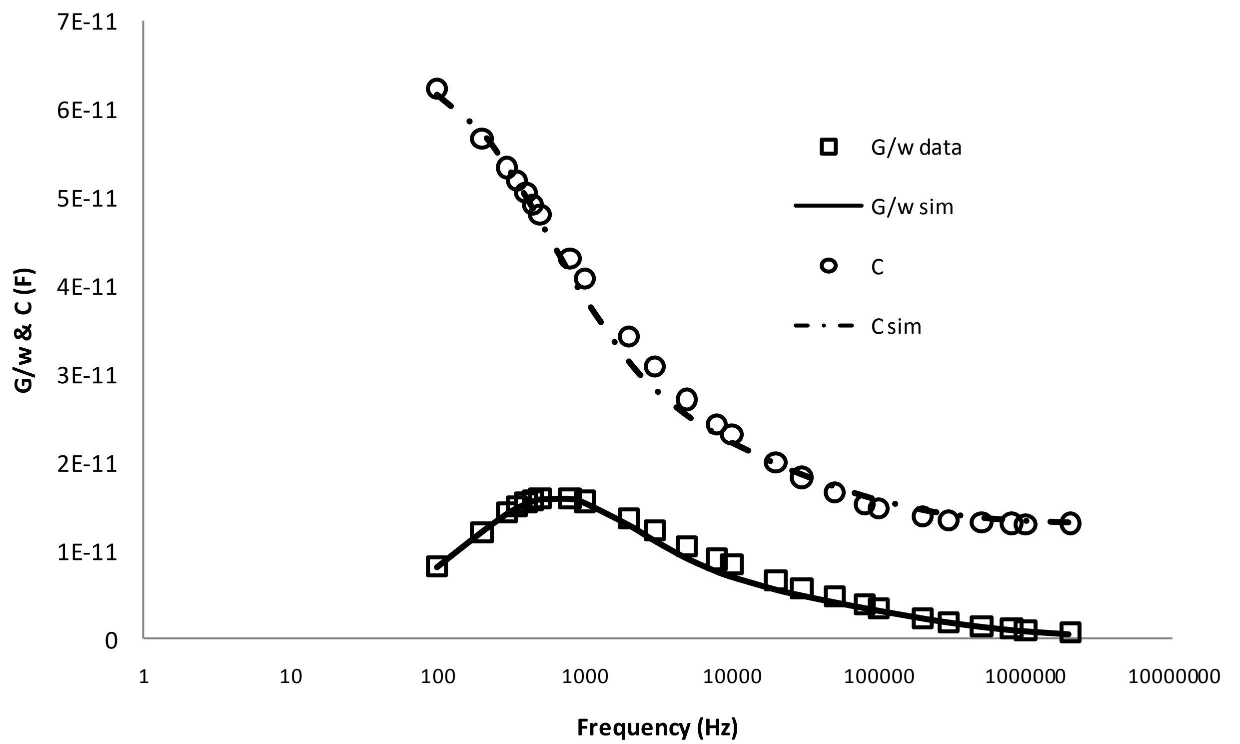

Figure 4.3: Measured and simulated C and G/ω as a function of frequency taken at 100V. Simulation assumed two main trap levels.

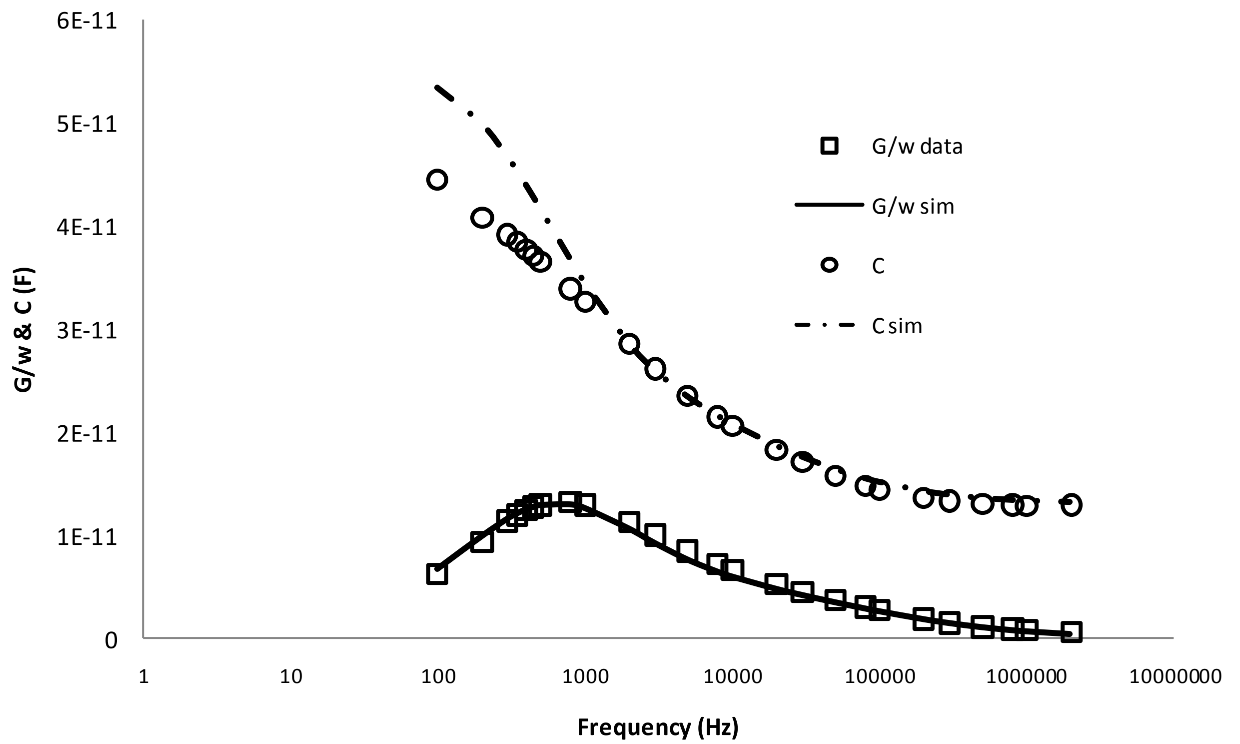

Figure 4.4: Measured and simulated C and G/ω as a function of frequency taken at 200V. The low frequency capacitance measurement is lower than expected

5 Irradiated Detector Results

Admittance measurements were taken on a several irradiated detectors. Conductance and Capacitance curves were simulated using the method described above. Figure 4.3 displays the measured and simulated admittance curves taken at a bias of 100V at a temperature of T=292 K on a p-on-n FZ detector. The simulation was produced assuming two trap levels, where one trap dominated the curves and the other contributed much less, but was necessary to include to correctly explain the data. There is good agreement between the simulation and the measurements, indicating that admittance measurements reveal important information for trap levels. Although our model agrees well with data at 100 V or below, the low frequency capacitance at higher voltages is smaller that predicted, as illustrated in Figure 4.4. It is not yet know the reason for the discrepancy, though an unknown contribution from the DC current is suspected Therefore, the conductance measurements were used to extract trap parameters and depletion depths.

The depth of the space charge region as a function of voltage for several diode detectors of different types, irradiation, and fluences was calculated using equation (4.34). Since the amount of charge collected from a trip sensor should be proportional to the active depth of the device, Charge Collection measurements are compared to the depleted depth for one p-on-n FZ pion, Figure 5.1, and one n-on-p MCz neutron, Figure 5.2, irradiated detector and good agreement is observed. The extracted depth for various neutron sensors is displayed in Figure 5.3 and for various pion sensors in Figure 5.4.

Deep level parameters for the most dominant deep level were extracted and presented in Table

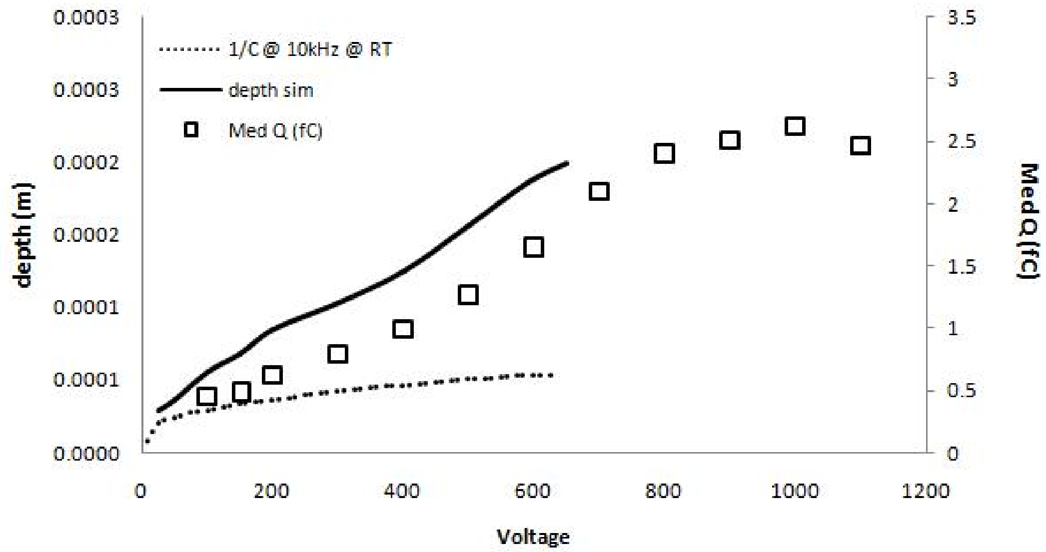

Figure 5.1: Extracted depletion region depth of a p-on-n FZ diode irradiated to 4.2E+14 pions/cm^2 and Median Charge of a p-on-n FZ strip detector irradiated to 6.0E+14 pions/cm^2. Also included is the depth calculated using the 10kHz capacitance.

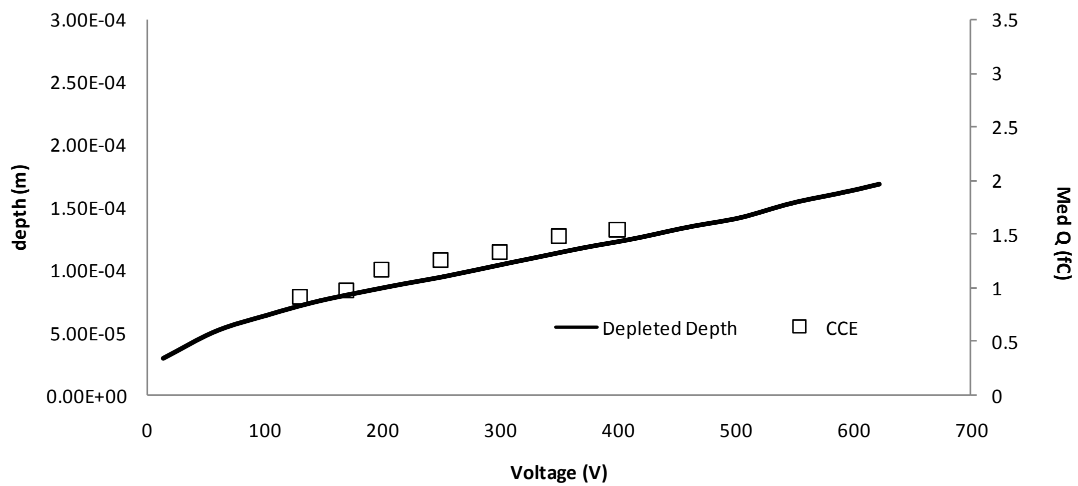

Figure 5.2: Extracted depletion region depth of a n-on-p MCz diode irradiated to 5E+14 neutrons/cm^2 and Median Charge of a n-on-p MCz strip detector irradiated to 5E+14 neutrons/cm^2

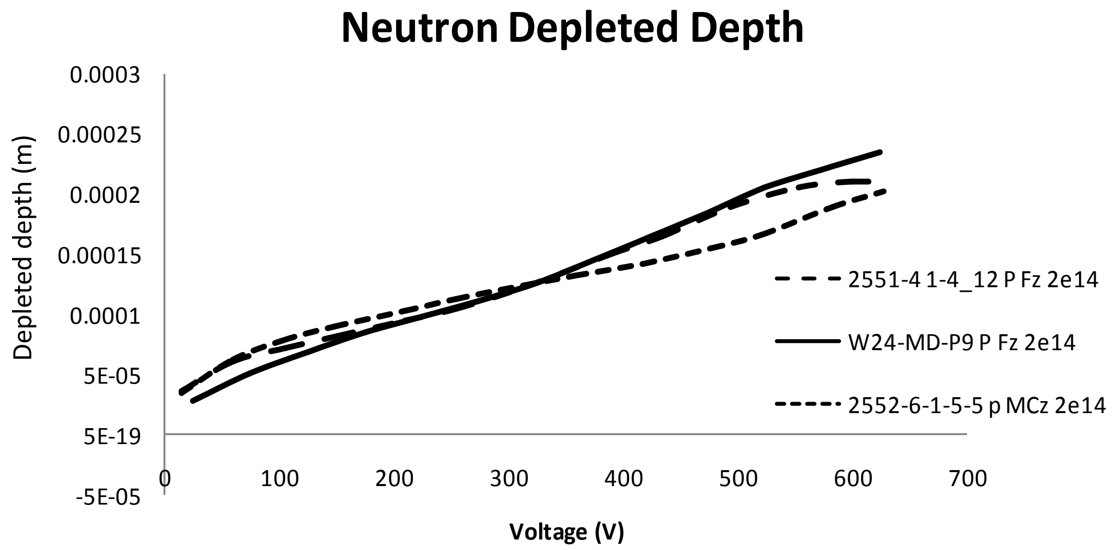

Figure 5.3: Depletion region depth as a function of voltage for neutron irradiated detectors, calculated using equation (4.34)

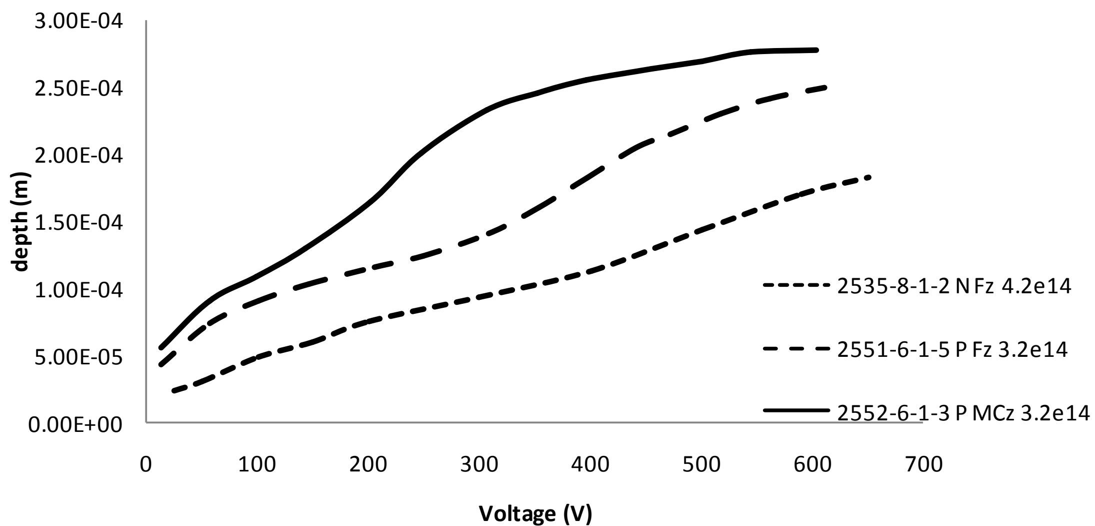

Figure 5.4: Depletion region depth as a function of voltage for pion irradiated detectors, calculated using equation (4.34)

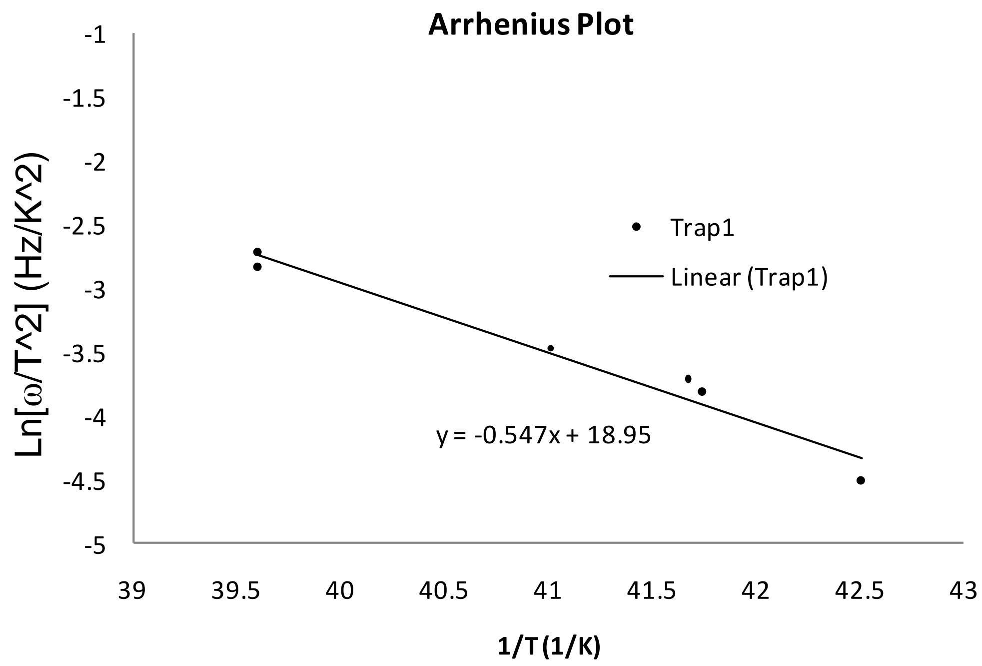

Figure 5.5: Arrhenius Plot for the dominant trap level. Activation energy was found to be E=.547 eV below the conduction band

Table 5.1: Deep Level Parameters

Pion Detector	Fluence	$N_{act}(1/cm^3)$	$N_{eff}(1/cm^3)$	$E_t(eV)$	Capture Cross. (cm^2)
N on P MCz	$3.2*10^{14}$	$1.7*10^{13}$	$7.2*10^{12}$	-0.54	$7.7*10^{-15}$
N on P FZ	$3.2*10^{14}$	$2.7*10^{12}$	$7.9*10^{12}$	-0.55	$9.8*10^{-15}$
P on N FZ	$4.2*10^{14}$	$3.5*10^{12}$	$9.4*10^{12}$	-0.55	$8.7*10^{-15}$

Neut. Detector	Fluence	$N_{act}(1/cm^3)$	$N_{eff}(1/cm^3)$	$E_t(eV)$	Capture Cross. (cm^2)
N on P MCz	$5*10^{14}$	$7.2*10^{12}$	$1.09*10^{13}$	-0.56	$2.4*10^{-14}$
N on P FZ p-spray	$2*10^{14}$	$8.0*10^{11}$	$5.76*10^{12}$	-0.58	$4.*10^{-14}$
N on P FZ	$2*10^{14}$	$1.0*10^{12}$	$5.76*10^{12}$	-0.58	$4.20*10^{-14}$

5.1. Energy level, majority carrier capture cross section, active concentration at the crossover, and average concentration calculated from the depletion voltage are presented. All energies are taken with respect to the conduction band and are determined from an Arrhenius plot of the peak frequency, as shown in Figure 5.5. The energy of deep level is close to midgap as expected. The concentration of active deep levels at the depletion edge (N_{act}) is larger for pion than for neutron detectors, although the average density (taken from V_{dep}) seems to be higher for neutrons. Capture cross sections are larger for neutrons than for pions.

6 Conclusions and Summary

Capacitance measurements can be used to determine the effective charge in silicon detectors. In the case of un-irradiated devices, the are no deep levels present, and the analysis is simplified making it possible to easily solve Poisson's equation in two dimensions to account for the geometry of a silicon strip detector. The geometry of the detector, namely the strip width and pitch, create a small offset in the $1/C$ and $1/C^2$ curves which is referred to as "the foot". The voltage range of "the foot" can accurately be modeled with the two dimensional solution to Poisson's equation and the effective doping density can be determined by the slope of the $1/C^2$ curve.

In irradiated detectors, the analysis becomes a lot more difficult due to the introduction of deep levels within the silicon bandgap. The deep levels will interact with the conduction and valence bands to form a spatially non-uniform charge density arising from the steady state filling of the deep levels. The deep levels will also complicate matters by introducing a frequency dependence to the measured capacitance. The frequency response of the deep levels can be determined by constructing an equivalent circuit that takes into account generation and recombination through a deep levels as well as any effect that free carriers have on the device. Admittance measurements, in particular the conductance, can be used to correct the frequency dependence of the measured capacitance, and the depth of the space charge region as a function of voltage can be extracted.

Once the admittance is modeled using equations (4.40) and (4.41), deep level parameters can be extracted from fitting the model to the data. The amplitude of the peak in the G/ω is directly

proportional to both the depletion capacitance and the number of active deep levels within a few kT of the Fermi level, so once C_d is known, N_{act} can be calculated using equation (4.32). The energy E_t of the deep level can be determined from the temperature dependence of the peak frequency ω_p by taking the slope of the Arrhenius plot. Once the energy is known, it can be plugged into equation (4.42) along with ω_p to determine the majority carrier capture cross section.

Although the method described in this paper gives a good idea of the concentration of deep levels, it is not sensitive to the charge of the deep levels. This means that type of deep level, donor or acceptor, cannot be known by this method alone, and must be inferred by other measurements. One possibility is to look for inversion from CCE measurements, and then determine that the dominant deep level must be of opposite type as the original if inversion occurs.

This method is also insensitive to the presence of a double junction that may arise in irradiated devices [9]. Only one junction is assumed in the analysis above, but this method can still be of use in a double junction model. Although this method cannot determine the presence of a double junction, the capacitance $C_d(V)$ is the capacitance across the entire space charge region, which includes both junctions if a double junction exists. This means that the total depleted depth $d(V)$ is the sum of depths of both junctions in the case of a double junction. This is due to the fact that free charge carriers are sampling the entire device when they fill and empty the deep levels.

Since good agreement is observed when the space charge depth determined from equation (4.34) is compared to the collected charge of a corresponding detector, this indicates that both sensors are depleting from the front side. If any of these have gone through type inversion, it could imply presence of a double junction citeEremin. The good agreement between the corrected depth and charge collection also gives shows that corrected C-V is a good indicator of collected charge as a function of voltage for detectors as long as inversion has not occurred. This could eliminate the need to measure collected charge in many cases, and instead perform a much simpler C-V measurement in its place.

In principal, the electric field within the an irradiated detector can be determined from the

above considerations. This analysis does not go that far, as the possibility of a double junction complicates the situation since the model presented in this paper assumes a single junction depleting from only one side of the detector.

Bibliography

[1] M.K. Petterson et al., "Determination of the Charge Collection Efficiency in Neutron Irradiated Silicon Detectors", SCIPP Preprints SCIPP 08/09

[2] M.K. Petterson, et al., RRESMDD06, Nucl. Inst. Meth. A (2007), doi:10.1016/j.nima.2007.08.222

[3] I.E. Anokhin, O.S. Zinets, Nuc. Inst. and Meth., Vol 477 1-3, Jan 2002

[4] R. Sonnenblick, "A Two Dimensional Simulation of a Silicon Microstrip Detector", Senior Thesis (1990) SCIPP 90/21

[5] S.M. Sze, "Physics of Semiconductor Devices", 2nd edition (1981)

[6] E. H. Nicollian and J.R. Brews, "MOS (Metal Oxide Semiconductor) Physics and Technology", 2003

[7] M. Beguwala and C. R. Crowell, "Characterization of Multiple Deep Level Systems in Semiconductor Junctions by Admittance Measurements", Solid-State Electronics, (1974), Vol.1 7, pp. 203-214

[8] M. P. Verkhovodov, H. P. Peka, D. A. Pulemyotov, "Capacitance Behavior of Junctions with Frozen Dopant Levels", Semicond. Sci. Technol., Vol. 8 1842-1847 (1993)

[9] V. Eremin, E. Verbitskaya, Z. Li, "Origin of the Double Peak Electric Field Distribution in Heavily Irradiated Silicon Detectors", Nucl. Inst. Meth. A 476 (2002) 556-554